Original Article

Effective Connectivity-based Unsupervised Channel Selection Method for Electroencephalography

Neda Abdollahpour[1], Nabi Sertac Artan[1], Ian Daly[2], Mohammadreza Yazdchi[3], Zahra Baharlouei[4]

[1]Department of Electrical and Computer Engineering, New York Institute of Technology, New York, NY, USA, [2]Department of Electrical Engineering, University of Essex, Colchester, Essex, UK, [3]Department of Biomedical Engineering, University of Isfahan, Isfahan, Iran, [4]Medical Image and Signal Processing Research Center, School of Advanced Technologies in Medicine, Isfahan University of Medical Sciences, Isfahan, Iran

Abstract

Background: Analyzing neural data such as Electroencephalography (EEG) data often involves dealing with high-dimensional datasets, where not all channels provide equally meaningful information. Selecting the most relevant channels is crucial for improving computational efficiency and ensuring robust insights into neural dynamics. **Method:** This study introduces the *Importance of Channels based on Effective Connectivity* (ICEC) criterion for quantifying effective connectivity (EC) in each channel. Effective connectivity refers to the causal influence one neural region exerts over another, providing insights into the directional flow of information. Using this criterion, we propose an unsupervised channel selection method that accounts for the intensity of interactions among channels. **Results:** To evaluate the proposed channel selection method, we applied it to three well-known EEG datasets across four categories. The assessment involved calculating the ICEC criterion using five effective connectivity metrics: partial directed coherence (PDC), generalized PDC (GPDC), renormalized PDC (RPDC), directed transfer function (DTF), and direct DTF (dDTF). To focus on the effect of channel selection, we employed the Common Spatial Pattern (CSP) algorithm for feature extraction and a Support Vector Machine (SVM) for classification across all participants. We compared our results against other CSP-based methods. The evaluation included comparing participant-specific accuracies with and without the proposed method across five effective connectivity metrics. **Conclusion:** The results showed consistent improvements and a significant reduction in the number of electrodes selected for all participants. Compared to state-of-the-art methods, our approach achieved the highest accuracies: 82% (13 out of 22 channels), 86.01% (29 out of 59 channels), and 87.56% (48 out of 118 channels) across all three datasets.

Keywords: *Brain connectivity, channel selection, effective connectivity, neuroimaging*

Submitted: 03-Jun-2025 **Revised:** 17-Sep-2025 **Accepted:** 25-Sep-2025 **Published:** 08-May-2026

Introduction

Electroencephalography (EEG) is a widely used neurophysiological technique for monitoring brain activity due to its noninvasive nature, affordability, and high temporal resolution. Although EEG is primarily categorized as an electrophysiological method rather than a structural imaging modality, it is often considered a form of functional neuroimaging because of its ability to capture dynamic brain processes in real time. EEG has become indispensable in numerous domains, including brain–computer interfaces (BCIs), cognitive neuroscience, and the diagnosis of neurological and psychiatric conditions.[1-3] In recent years, its role in biomedical research and clinical practice, especially for diagnosing and treating brain disorders, has grown significantly.[4-6]

A fundamental challenge in EEG-based analysis is the high dimensionality of multichannel recordings, which can increase computational burden and hinder real-time processing.[3] Consequently, effective channel selection has emerged as a crucial preprocessing step. By identifying and retaining only the most informative EEG channels, channel selection not only reduces data dimensionality and computational complexity but also enhances classification performance and practical usability.[7] For instance, in motor imagery (MI)-based BCIs for individuals with paralysis, selecting a minimal yet informative subset of electrodes can alleviate user fatigue and improve system efficiency.

How to cite this article: Abdollahpour N, Artan NS, Daly I, Yazdchi M, Baharlouei Z. Effective connectivity-based unsupervised channel selection method for electroencephalography. J Med Signals Sens 2026;16:11.

Address for correspondence:
Dr. Zahra Baharlouei, Medical Image and Signal Processing Research Center, School of Advanced Technologies in Medicine, Isfahan University of Medical Sciences, Isfahan, Iran.
E-mail: zahra.bahar@res.mui.ac.ir

Access this article online

Website: www.jmssjournal.net

DOI: 10.4103/jmss.jmss_55_25

Quick Response Code:

Existing channel selection methods are typically classified into three main categories: filter-based, wrapper-based, and hybrid approaches.[7-10] Filter-based methods evaluate channels using statistical measures or information-theoretic criteria independently of any classifier. These methods are computationally efficient and scalable but may overlook task-specific discriminative power, resulting in suboptimal performance.[7] In contrast, wrapper-based methods assess subsets of channels based on their impact on classification accuracy through iterative training and validation. While these methods often yield higher performance, they are prone to overfitting and require substantial computational resources.[9] Hybrid approaches attempt to combine the strengths of both paradigms to achieve a balance between efficiency and accuracy.[10,20]

However, beyond identifying which channels are statistically relevant, understanding how brain regions communicate during cognitive tasks such as MI is equally important. Traditional channel selection approaches often neglect the dynamic, directed nature of neural interactions. In this context, effective connectivity (EC) offers a powerful framework by quantifying the causal influence that one brain region exerts over another.[11,36] Unlike functional connectivity (FC), which captures only undirected correlations, EC models the directional flow of information, uncovering the mechanistic basis of inter-regional communication.[22] This is especially valuable in MI tasks, where communication patterns between motor, sensory, and associative cortices vary across individuals.[12] By leveraging EC, researchers can identify EEG channels that correspond to brain regions exhibiting the most significant task-related causal interactions. This not only supports participant-specific channel selection but also enhances interpretability and neurophysiological validity.[13]

Previous studies

A variety of EEG channel selection techniques have been proposed to improve classification performance and reduce computational load in BCI systems, particularly in MI tasks. These approaches can be broadly categorized into filter-based, wrapper-based, and hybrid methods.

Filter-based methods rank channels independently of the classifier using statistical, frequency, or information-theoretic measures. For example, Gaur *et al*.[15] introduced a multiclass classification framework using multivariate empirical mode decomposition to decompose EEG signals into intrinsic mode functions, followed by filtering based on mean frequency. This method captures dominant rhythms such as μ and β without any classifier involvement. While computationally efficient and interpretable, such methods may neglect the interaction between selected channels and classification accuracy.

In contrast, wrapper-based methods rely on iterative classifier training and evaluation to search for an optimal subset of channels. Jin *et al*.[14] proposed the bispectrum-based channel selection method (BCS-common spatial pattern [CSP]), which extracts nonlinear coupling features such as the sum of logarithmic amplitudes and the first-order spectral moment from bispectrum analysis. The features are then evaluated through CSP and classification, making this a wrapper-based method. Similarly, Qiu *et al*.[17] used an improved sequential forward floating selection (SFFS) algorithm that evaluates classification performance at each iteration to retain the most relevant channels. These methods are often more accurate but come with high computational overhead and carry the risk of potential overfitting.

Some studies adopt hybrid approaches to balance accuracy and efficiency. Esfahani *et al*.[34] used a multiobjective optimization strategy combining regularized CSP with Strength Pareto Evolutionary Algorithm II to simultaneously optimize classification accuracy and the number of selected channels. This represents a hybrid method since it integrates CSP-based spatial filtering (typically filter-based) with classifier-driven evaluation. Likewise, Arvaneh *et al*.[18] optimized both channel selection and classification in a joint framework using information gain and classifier feedback, highlighting the advantages of combining both paradigms.

Other notable wrapper-based approaches include Tiwari and Chaturvedi's dynamic channel relevance method,[19] which updates the importance of channels based on classification feedback in real-time, and the binary gravitational search algorithm (IBGSA) applied by Ghaemi *et al*.,[33] which evolves a population of channel subsets guided by classification performance. Raza *et al*.[16] took a different approach by incorporating adaptive learning through covariate shift detection, although their framework still relied on supervised feedback for channel relevance.

Despite their contributions, most existing methods focus primarily on statistical or frequency-domain criteria without explicitly modeling the underlying neural mechanisms. They treat EEG channels as isolated signals rather than as components of a dynamic network. In tasks like MI, where task-specific brain regions (e.g., motor, sensory, and premotor cortices) interact differently across individuals, the absence of a neurophysiologically grounded framework limits the generalizability and interpretability of channel selection strategies.

Crucially, none of the methods discussed incorporate EC, which captures the directional and causal influence among neural regions, as a basis for channel selection. EC provides a mechanistic understanding of information flow between brain areas and has the potential to identify channels most relevant to task-related neural dynamics. By integrating EC analysis into the channel selection process, our proposed method not only reduces dimensionality but also aligns selected channels with meaningful brain–region interactions, offering both computational and neuroscientific advantages.

Research gap and objectives

Despite significant progress in EEG channel selection for MI-based BCI systems, existing methods often fall short in achieving a balance between accuracy, computational efficiency, and neurophysiological interpretability. Wrapper-based approaches typically involve iterative retraining with classifiers, which increases the computational burden and risks overfitting, particularly when the EEG data are high-dimensional or limited in size. In contrast, filter-based methods rely on signal statistics for selection, offering scalability but often lacking task adaptability and classifier feedback. Hybrid methods attempt to bridge the gap but still frequently overlook participant-specific neural dynamics and apply uniform selection strategies across participants.

Crucially, most of these approaches treat EEG channels as isolated inputs rather than nodes within a dynamic neural network, ignoring the brain's causal communication patterns during MI. They rarely incorporate EC, which models the directional influence among brain regions and has the potential to inform more functionally meaningful channel selection. This leads us to the central research question of this study:

Can EEG channel selection be improved by leveraging individualized EC patterns to adaptively identify participant-specific and functionally relevant channels for MI classification?

To answer this, we propose a novel unsupervised channel selection framework based on individualized EC analysis. Our objectives are to (1) model directed inter-regional interactions to guide channel selection, (2) adapt the selection for each participant and frequency band, and (3) benchmark our proposed method against traditional selection strategies in terms of accuracy, computational efficiency, and neurophysiological relevance.

Our proposed method is notable for its simplicity, versatility, and efficiency: it significantly reduces data dimensionality while maintaining strong classification performance, operates without requiring labeled data, and supports broad applicability across different modalities and tasks. Moreover, it is compatible with both resting-state and event-related designs and has the capacity for visualization, enhancing its utility in diverse neuroimaging contexts.[35]

This paper is structured as follows: Section 2 presents the mathematical concepts underlying the study, including EC metrics, model order determination, and Vector Autoregression (VAR) model validation. Section 3 details our proposed methodology, covering data descriptions, the importance of channels based on EC (ICEC)-based channel selection process, feature extraction, and the overall framework. Section 4 provides a comprehensive evaluation of the method, including its impact on classification, comparisons with existing approaches, computational efficiency, and potential applications. Finally, Section 5 concludes the paper with a summary of findings and future research directions.

Mathematical Concepts

In this section, we provide a brief overview of the mathematical formulations of the types of EC and the autoregressive model used in this study to aid understanding.

A statistical concept of causality is provided by Granger causality.[21] According to this concept, if a signal Y_1 "Granger-causes" (or "G-causes") a signal Y_2, then past values of Y_1 should contain information that helps predict Y_2 above and beyond the information of the past values of Y_2 alone. The mathematical formulation of the method is based on linear regression modeling of stochastic processes.[21] The evaluation of causal interactions among various brain regions is fundamental to elucidating their functional operations. A promising way to identify such links is using multivariate autoregressive (MVAR) modeling methods, which are applied to multisite electrophysiological recordings. Indeed, they can estimate the extent to which past activity in one or more brain regions can predict current activity in another while taking into account the mediating effects of others.[22,23]

Effective connectivity metrics

An extension of Granger causality is partial directed coherence (PDC), which normalizes terms in the frequency domain by the total outflow at a node. Directed transfer function (DTF), on the other hand, normalizes frequency-domain terms by the total inflow at a node. This is an alternative causal model that normalizes directed effects by the sum of the transfer functions going into the node, as opposed to the sum of the transfer functions going out of the node as measured by the PDC.[22,24]

Given the MVAR model in Eq. 1, the system is defined with a model order ρ, which specifies the number of past time points (lags) used to predict the current state of the EEG signals. In this formulation, X(t) represents the multichannel EEG signal vector at time t, where each element corresponds to a recording channel. The term E(t) denotes the residual error vector, capturing the portion of the signal that is not explained by its past values, essentially representing noise or new, unpredicted activity.

$$X(t)=\sum_{k=1}^{\rho}A^{(k)}(t)X(t-k)+E(t) \quad (1)$$

Eq. 2 introduces A(f, t), the frequency-domain system matrix, which is computed by applying a Fourier transform to the time-domain MVAR coefficients $A^{(k)}$. These coefficients describe the linear relationships between the channels at various time lags k. The identity matrix $A^{(0)} = I$ ensures that the model includes the current value of the signal vector as a baseline reference.

$$A(f,t)=-\sum_{k=0}^{\rho}A^{(k)}(t)e^{-i2\pi fk};A^{(0)}=I \quad (2)$$

Eq. 3 expresses the model in the frequency domain, where X(f,t) and E(f,t) are the Fourier transforms of the time-domain EEG signal and residuals, respectively. The matrix H(f,t) is referred to as the transfer function. It captures how input components (residuals) at different frequencies propagate through the modeled system to produce the observed outputs. This transfer function plays a central role in the computation of frequency-based EC measures used in subsequent analysis.

$$X(f,t)=A(f,t)^{-1}E(f,t)=H(f,t)E(f,t) \quad (3)$$

The DTF is then formulated as shown in Eq. 4. In this equation, ηij2(f) represents the normalized measure of directional influence from channel j to channel i at a specific frequency f. The term $|H_{ij}(f)|^2$ is the squared magnitude of the element in the transfer function matrix H(*f*), which quantifies how strongly the activity in channel j contributes to the signal observed in channel I at frequency f.

The denominator, $\sum_{k=1}^{M}|H_{ik}(f)|^2$ sums the squared magnitudes of all incoming influences to channel i from all other channels k (where M is the total number of channels or variables). This normalization ensures that the DTF values are relative and allow comparisons across connections. The resulting ratio provides a frequency-specific estimate of the strength of the directional interaction from channel j to channel i, relative to all sources affecting channel i. This formulation is valid for systems with more than two variables (M > 2).[22,25-27]

$$\eta_{ij}^2(f)=\frac{|H_{ij}(f)|^2}{\sum_f\sum_{k=1}^{M}|H_{ik}(f)|^2};M>2 \quad (4)$$

From the DTF, the direct DTF (dDTF) is computed as shown in Eq. 5. In this expression, $\delta_{ij}^2(f)$ combines two components: $\eta_{ij}^2(f)$, which is the ffDTF, and $P_{ij}^2(f)$, the partial coherence between channels i and j at frequency f. The multiplication of these terms enhances the specificity of directional interactions by emphasizing those that are both strong interactions.

$$\delta_{ij}^2(f)=\eta_{ij}^2(f)P_{ij}^2(f) \quad (5)$$

Eq. 6 defines the PDC, $\Pi_{ij}^2(f)$, which measures the direct influence of channel j on channel i in the frequency domain. This is calculated using the squared modulus of the frequency-domain coefficient $A_{ij}(f)$, normalized by the total output influence from channel j across all connections.

$$\Pi_{ij}^2(f)=\frac{|A_{ij}(f)|^2}{\sum_{k=1}^{M}|A_{kj}(f)|^2} \quad (6)$$

The generalized PDC (GPDC), shown in Eq. 7 and denoted as $\bar{\pi}_{ij}(f)$, extends PDC by incorporating a normalization factor related to the noise covariance. This ensures that the measure is scale invariant and allows for comparisons across different signal magnitudes. The formulation is constrained such that the squared magnitude of $\bar{\pi}_{ij}(f)$ lies between 0 and 1, and the sum of all outflow magnitudes from a source node j equals 1 across all destinations i.

$$\bar{\pi}_{ij}(f)=\frac{\frac{1}{\sum_{ii}A_{ij}(f)}}{\sqrt{\sum_{k=1}^{M}\frac{1}{\sum_{ii}|A_{kj}(f)|^2}}} \quad (7)$$

$$0\le|\bar{\pi}_{ij}(f)|^2\le1;\sum_{j=1}^{M}|\bar{\pi}_{ij}(f)|^2=1$$

Renormalized PDC (RPDC) $\lambda_{ij}(f)$, introduced in Eq. 8, is computed by projecting the vector $Q_{ij}(f)$, composed of the real and imaginary parts of the coefficient $A_{ij}(f)$ (as shown in Eq. 9), onto a covariance-weighted space.

$$\lambda_{ij}(f)=Q_{ij}(f)\times V_{ij}(f)^{-1}Q_{ij}(f) \quad (8)$$

$$Q_{ij}(f)=\begin{pmatrix}\mathrm{Re}[A_{ij}(f)]\\ \mathrm{Im}[A_{ij}(f)]\end{pmatrix} \quad (9)$$

The matrix $V_{ij}(f)$, defined in Eq. 10, incorporates both the inverse of the autocovariance structure R_{jj}^{-1} and the noise covariance Σ_{ii}, weighted by the trigonometric matrix $Z(\omega,k,l)$ (Eq. 11). The matrix R represents the full covariance matrix of the VAR[ρ] process and has dimensions $(M\rho)^2\times(M\rho)^2$, where M is the number of EEG channels and ρ is the model order. These components together allow RPDC to account for uncertainty and provide a robust measure of directed connectivity.

$$V_{ij}(f)=\sum_{k,l=1}^{\rho}R_{jj}^{-1}(k,l)\Sigma_{ii}Z(2\pi f,k,l) \quad (10)$$

$$Z(\omega,k,l)=\begin{pmatrix}\cos(\omega k)\cos(\omega l) & \cos(\omega k)\sin(\omega l)\\ \sin(\omega k)\cos(\omega l) & \sin(\omega k)\sin(\omega l)\end{pmatrix} \quad (11)$$

Where R is the $[(M\rho)^2\times(M\rho)^2]$ covariance matrix of the VAR[ρ] process, a vector autoregression of order ρ.[22,28]

In the proposed method, the MVAR model is applied to each trial to estimate directed relationships among EEG channels. The MVAR coefficients form the foundation for calculating frequency-domain EC metrics, including DTF, dDTF, PDC, GPDC, and RPDC. The model order ρ, which determines how many past time points are used for prediction, is selected individually for each trial using Akaike's information criterion (AIC), explained in Section 2.2. This approach ensures that the model captures the essential temporal dependencies while minimizing overfitting. The extracted connectivity matrices are then used as input features for the subsequent classification pipeline.

Model order

Model order (ρ) assumes a pivotal role in fitting an MVAR model. Indeed, the quality of model fitting is contingent on

the order of the model. Model orders that are too small or too large can result in spectra that lack the necessary detail or create spurious maxima in the corresponding spectrum, respectively.[22,27] To determine the optimum order of the model, different criteria such as AIC, Hannan–Quinn's criterion, and Bayesian–Schwartz's information criterion have been proposed.[22] In this study, we used the AIC method, which is the most preferred method to find the proper model order. AIC is calculated as

$$\mathrm{AIC}(\rho)=\ln\left(|\det(V)|\right)+\frac{2}{N}\rho K^2 \quad (12)$$

In Eq. 12, V denotes the residual noise covariance matrix, and E(t) represents the time-varying error term. The first term, ln(|det(*V*)|), reflects the logarithmic determinant of the estimated residual covariance matrix V(ρ), which varies with the model order ρ. This term captures how well the model fits the data. The second term, $\frac{2}{N}\rho K^2$, serves as a complexity penalty, where K is the number of channels (or variables), and N is the total number of observations. This term discourages overfitting by penalizing models with higher complexity.[22,25]

VAR model validation

There are a number of criteria we can use to determine whether we are fitting our VAR model appropriately. Three commonly used categories of tests are Whiteness tests for checking the residuals of the model for serial and cross-correlation, Consistency tests to evaluate whether the model generates data with the same correlation structure as the real data, and the Stability test to check the stability/stationarity of the model.[22] In this study, we selected a model order for the multivariate VAR model that satisfied the stability criterion for all samples, ensuring it was specific to each participant. This means that for each participant, we determined the appropriate model order that maintained the stability of the MVAR model across all their respective data samples. By doing so, we ensured that the fitted MVAR models were both participant-specific and stable, which is crucial for accurate analysis of brain connectivity.

Methodology

In this section, we introduce our proposed EEG channel selection method. We describe datasets, the main steps of the proposed method, and its formulation.

Data descriptions

Dataset 1

We use dataset 2a from the BCI-Competition IV,[29] 2008. This is a four-class MI BCI dataset. It contains EEG signals from 9 healthy participants who performed 4 different MI tasks (imagining the movement of the left hand, right hand, leg, and tongue). Each dataset contains 288 labeled trials (training data), 72 trials per class, and 288 test trials. A detailed timeline of a single MI trial within this dataset is shown in Figure 1a. In this dataset, 22 EEG electrodes were used to record brain signals, and the sample rate of the EEG is 250 Hz. The position of the electrodes is based on the international EEG 10–20 systems.

Dataset 2

We use dataset 1 from the BCI-Competition IV.[30] This is a two-class MI BCI dataset. It contains MI EEG signals from 7 participants. However, we eliminated participants "c", "d", and "e" as they were generated artificially and assessed only the remaining participants. During the first two runs, arrows pointing left, right, or down were presented as visual cues on a computer screen for 4 s. During this time span, each participant was instructed to perform the cued MI task, followed by 4 runs with unequal time periods of MI trials ranging from 1.5 to 8 s. The timeline of every MI trial is shown in Figure 1b. In this dataset, 59 EEG electrodes were used to record brain signals, and the sample rate of the signals is 1000 Hz, which was downsampled to 100 Hz.

Dataset 3

We use dataset IVa, BCI-Competition III.[31] This is a two-class MI BCI dataset with small training sets. It contains MI EEG signals recorded from five healthy participants: *aa*, *al*, *av*, *aw*, and *ay*. Each participant performed 280 MI tasks containing train and test trials.

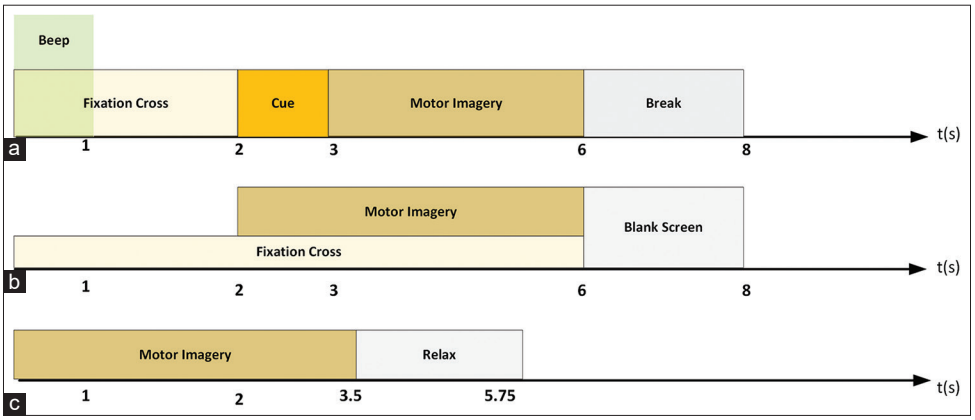

Figure 1: Timeline of each trial for dataset 1 (a), dataset 2 (b) and dataset 3 (c)

The number of train and test trials is not equal for all participants. In each run, there are 3.5-second visual cues for the three MI tasks the participant is asked to perform: (L) left hand, (R) right hand, and (F) right foot. In this dataset, 118 EEG electrodes were used to record brain signals, and the sample rate of the signals is 100 Hz. The timeline of every MI trial is shown in Figure 1c.

Proposed method

Acquiring 4-D effective connectivity matrices

To acquire 4-dimensional EC matrices, we used EEGLAB Toolbox[32] (version 2021.1) and MATLAB (version R2018b). The only preprocessing applied to the datasets was band-pass filtering the signal to the 1–40 Hz interval using a fifth-order Butterworth filter. In this study, we used 1000, 750, 400, and 250 time points for dataset 1 (4-class), dataset 1 (2-class), dataset 2, and dataset 3, respectively. These were selected to align with the specific requirements and structures of each dataset, ensuring that the selected time range accurately captured the MI tasks within each experimental framework. Then, the model was preprocessed by normalizing trials across time (method: ensemble) for each participant.

In this study, the model order was determined using AIC. To ensure the stability of the MVAR model, the selected order was adjusted across trials for each participant until the stability criterion was satisfied.[22] The MVAR model was then fitted using a sliding window approach, with a window length of 0.5 s and a step size of 0.03 s. Finally, EC measures were computed from each window across the frequency range of 1–40 Hz.

In the next stage, we calculated ICEC measures. To assess EC across different neural frequency bands, we computed frequency-specific connectivity matrices for each EC metric. Specifically, seven distinct frequency ranges were considered: Theta (4–7 Hz), Mu (8–12 Hz), low-beta (13–15 Hz), high-beta (18–30 Hz), 29–40 Hz, 8–30 Hz, and 1–40 Hz. For each frequency band and each EC type (DTF, dDTF, PDC, GPDC, and RPDC), we generated a 4-dimensional matrix with dimensions corresponding to sink channels, source channels, frequency bins, and time windows. As a result, each participant had 35 EC matrices (5 EC types × 7 frequency bands), capturing the dynamic and spectral characteristics of directed connectivity over time.

Calculating the importance of channels based on effective connectivity

Figure 2 outlines the 5 main steps for calculating the ICEC amount for each channel. As can be seen from the illustrations, in the first two steps, the dimensions of the input are reduced. In these stages, we use specific windows that determine the borders of the third (frequency) and the fourth (time) dimensions, respectively.

In this study, we use seven different windows for the third dimension (7 different frequency ranges). We use all time samples without applying a specific window. The result of

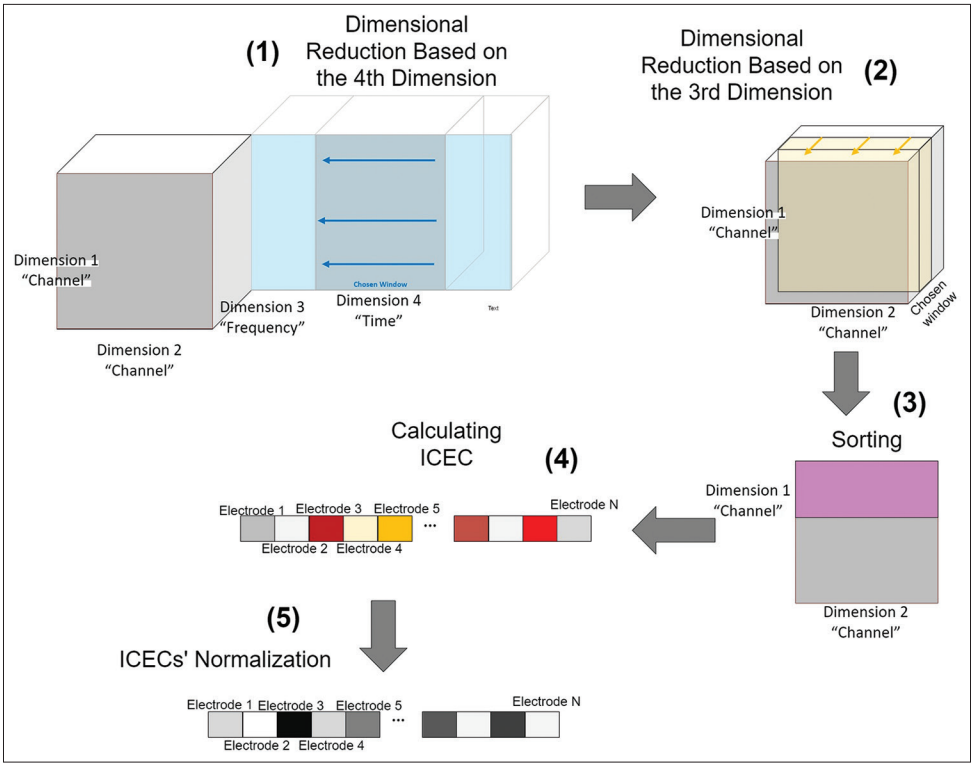

Figure 2: Five major steps for calculating the importance of each electrode: the first two steps reduce the dimensions of a 4D effective connectivity matrix for a participant, followed by sorting, importance of channels based on effective connectivity calculation, and normalization. ICEC – Importance of channels based on effective connectivity

the aforementioned stages is a square matrix ($N_{ch} \times N_{ch}$) where N_{ch} is the total number of electrodes for each task. Every value within this matrix can also be calculated by Eq. 13 using Algorithm 1.

$$C_{i\times j} = \frac{\sum_{f=f_{min}}^{f_{max}} \sum_{w=w_{min}}^{w_{max}} con_{i\times j\times f\times w}}{(w_{max} - w_{min})(f_{max} - f_{min})} \quad (13)$$

As for the $C_{i\times j}$ amounts, when is a 4-dimensional EC matrix; $C_{i\times j}$ is a measure that depicts the mean value of interactions between node *i* and *j*. Calculating $C_{i\times j}$ for all channels gives us a square matrix. After sorting $C_{i\times j}$ amounts within the matrix and summing up the 30% of the highest ones for each electrode, we possess ICEC for each EEG channel as a factor to evaluate the importance of each electrode. 30% was chosen by trial and error in this study. After normalizing the figures, in the last stage, we selected some subsets of electrodes considering their highest amounts of ICECs in a circle with the usage of a classifier to evaluate their suitability for aiding EEG decoding.

To avoid conflating different EC metrics, we computed "Con" separately for each EC measure and each frequency band. Specifically, for each participant, we obtained 35 distinct con tensors, corresponding to 5 EC measures (DTF, dDTF, PDC, GPDC, and RPDC) applied independently across the 7 frequency ranges. These tensors were not averaged, combined, or fused at any stage. This separation was crucial, as our aim was to explore how each frequency-specific EC pattern contributes uniquely to the ICEC computation and channel selection process, allowing for a more detailed and interpretable analysis of spectral connectivity profiles across participants.

Frequency ranges

In the process of calculating $C_{i\times j}$, we consider 7 different frequency ranges to assess the proposed model for each user. They are theta (4–7 Hz), Mu (8–12 Hz), low-beta (13–15 Hz), high-beta (18–30 Hz), 29–40 Hz, 8–30 Hz, and 1–40 Hz. There is also the possibility of selecting a particular period of time within the timeframe of a trial; however, in this study, we use all windows (time points) without any selection.

Time points and adaptive multivariate autoregressive details

In this study, we used adaptive MVAR (AMVAR) models trained with the Vieira–Morf algorithm,[22] for all participants. The model order amounts range from 15 to 40, depending on the size of the dataset selected for each user. In total, we use window lengths of 0.5 s and a window step size of 0.03 s for all users in the model fitting step.

The number of windows and time points (the 4th dimension of the 4-D EC matrices) are 90, 67, and 117 for all participants from dataset 1, 2, and 3, respectively (2-class tasks). The time points for dataset 1, considering all classes (a 4-class task), are also 126 for all 9 participants.

Algorithm 1: Effective Connectivity-based EEG.

Channel Selection

1. Read 4-D Effective Connectivity (labeled "con")
   $con \in R^{N_{Ch}\times N_{Ch}\times N_f \times N_w}$,
   N_f = *Number of specific frequencies chosen*
   N_w = *Number of windows* (*time points*),
   N_{Ch} = *Number of EEG channels*
2. For $i = 1 : N_{Ch}$ % "From" dimension
3. For $j = 1 : N_{Ch}$ % "To" dimension
4. While $i \neq j$
5. Calculate $C_{i\times j}$ according to Eq. (13)
   Construct matrix "Zs" containing $C_{i\times j}$ measures for all nodes
6. Break
7. End
8. End
9. End
10. Sort Zs measures based on the "From" dimension, "Zs" $Zs \in R^{N_{Ch}\times N_{Ch}}$
11. Calculate the sum of the 8 first amounts of Z_s, (labeled "M")
12. Sort M from the maximum amount to the minimum, "ICEC" and calculate the index and amount of ICEC for each electrode
    Index = Selected electrodes
    Amount = weight of each node (Normalized ICEC).

4-D effective connectivity matrices

In this study, we calculate 5 types of EC for each user to assess the proposed method and also to make a comparison of their effectiveness. The 4-D EC matrix dimensions are "to," "from," "frequency range," and "time," respectively. As the "to" and "from" dimensions are EEG channels, the 3rd dimension indicates the ranges of frequencies in which the interactions among nodes are evaluated. The 4th dimension also shows each aforementioned window as a time point.

Channel selection using the importance of channels based on effective connectivity

As can be seen within the algorithm, after extracting a user-dependent 4-D matrix, ICEC measures are calculated for each EEG channel in 7 different frequency ranges. After sorting these criteria measures and normalizing them, we select a subset of EEG channels with the highest amounts of ICEC. We evaluate our model by selecting electrodes ranging from 5 to a maximum of 22, 59, and 118 electrodes for datasets 1, 2, and 3, respectively.

Figure 3 depicts interactions based on RPDC measures, between two specific EEG electrodes (CP3 with a high ICEC amount and C6 with a low ICEC amount) and 4 other electrodes (P1, CP1, PZ, and C3) separately, (a)

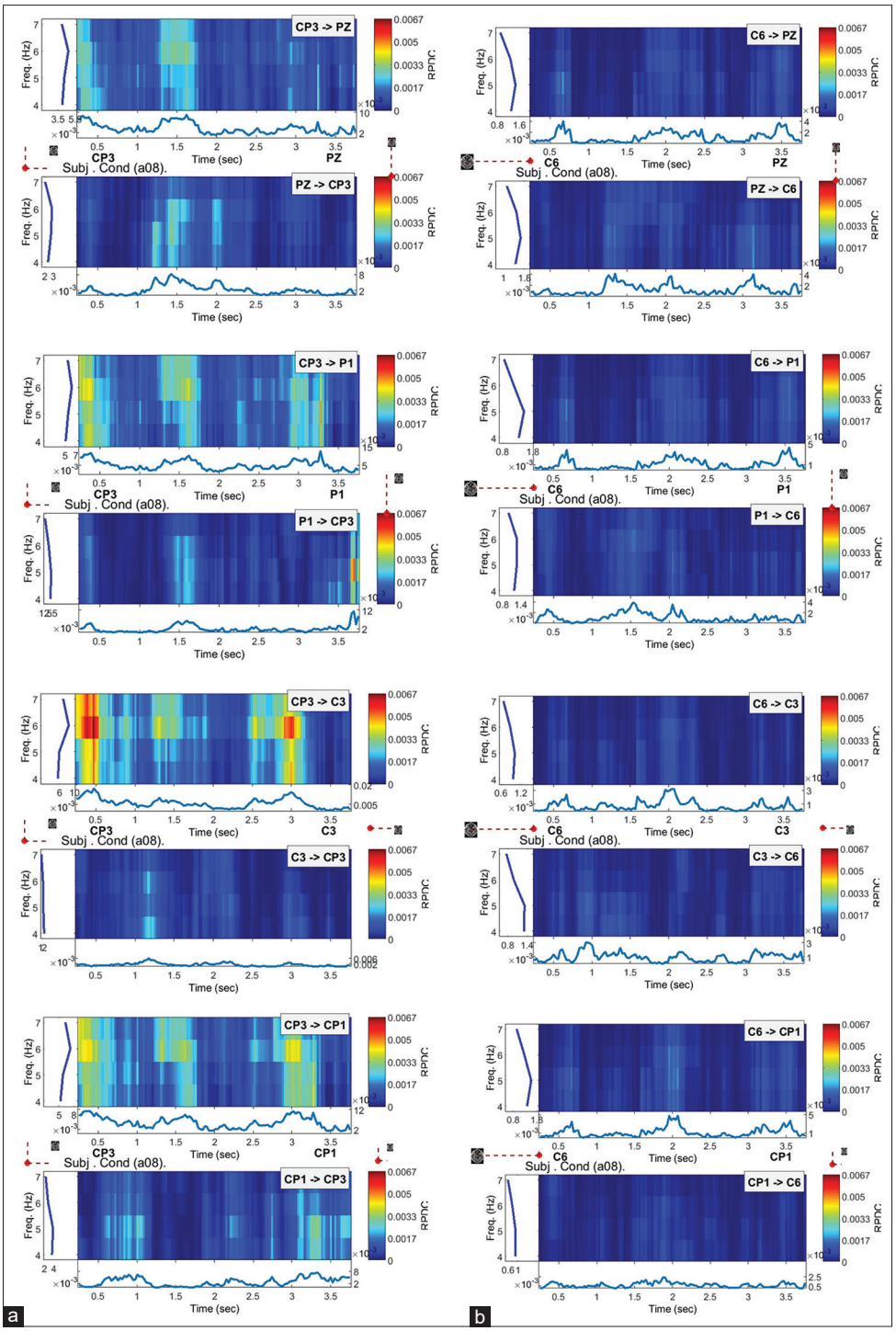

Figure 3: Comparison of renormalized partial directed coherence interactions for participant "a08" in dataset 1 between electrodes (a) C6 (low importance of channels based on effective connectivity [ICEC]) and (b) CP3 (high ICEC) with four other electrodes (P1, CP1, PZ, and C3)

and (b). We chose these channels randomly to compare their interactions with both a channel with a high ICEC value and a channel with a low ICEC value.

It is important to note that the channel selection process using ICEC is performed adaptively for each participant. Specifically, the 4-D EC matrices and the resulting ICEC values are calculated independently per participant, across multiple frequency bands and time windows. Consequently, the set of selected electrodes is tailored to each participant's unique connectivity patterns, ensuring that the selection is data-driven and context-specific rather than fixed or global.

Feature extraction

In the feature extraction stage, we employ the CSPs algorithm, which is a widely used spatial filtering technique in EEG signal processing. For binary classification

tasks (2-class problems), we use standard binary CSP, while for dataset 1, which involves a four-class MI task, we apply a one-versus-rest multiclass CSP approach. CSP works by finding spatial filters that maximize the variance of one class while minimizing the variance of the other, thereby enhancing class-discriminative EEG features. Specifically, for each pair of classes, CSP computes a projection matrix that transforms multichannel EEG data into a set of components whose variance patterns are most informative for distinguishing between the two classes.

After applying the CSP transformation, we calculate the variance of the projected signals for each trial. These variance features capture the distribution of EEG power across spatial patterns and serve as input features for classification. This process is repeated independently for each frequency band considered in our analysis, ensuring frequency-specific feature extraction. For example, when analyzing the mu frequency band (8–12 Hz), we first filter the data accordingly, then apply CSP, and finally compute the variance features within that frequency band.

In the classification stage, we use support vector machines (SVMs) with a radial basis function kernel. Binary SVMs are applied to all 2-class tasks, while a one-versus-the-rest strategy is used for both the multiclass CSP and multiclass SVM applied to dataset 1. The combination of CSP and SVM is well-suited for EEG classification tasks, offering a balance between discriminability and computational efficiency. By conducting the entire CSP and classification pipeline separately for each frequency band, we ensure that the extracted features are both spatially and spectrally informative.

Whole framework

The framework for evaluating the proposed EEG channel selection method for all datasets is the same and is shown in Figure 4. In the first stage, the preprocessing stage, the data are segmented into training and testing sets and filtered by a band-pass Butterworth filter with order 3 and between 8 and 30 Hz. Dataset 1 was segmented between 625 and 1374 time points for all users and for both 2-class and 4-class categories. In addition, 2.5 s (containing 250 samples) are segmented for all users of dataset 2, while 4 s (400 samples) are used for dataset 3.

Results and Discussions

Impact of channel selection on classification performance across subjects

In this study, we use 5 EC measures (DTF, dDTF, PDC, GPDC, and RPDC) to calculate the ICEC criterion. This criterion is also assessed through 7 different frequency ranges: theta, mu, low-beta, high-beta, gamma, 8–30 Hz, and 1–40 Hz for each participant.

Figure 5 presents the average accuracies across subjects for the four datasets evaluated in this study using the ICEC criterion. As shown in Figure 5, channel selection based on all types of EC metrics led to improved performance across datasets, with RPDC demonstrating particularly strong results. For instance, for dataset 2, the accuracy values for RPDC consistently exceeded 86%, while other metrics, such as GPDC and PDC, achieved accuracies in the range of 80%–85%. These findings underscore the effectiveness of the proposed method in enhancing classification performance through EC-based channel selection, with RPDC making the most significant contribution.

This is worth mentioning that the accuracy values reported in Figure 5 represent the overall mean performance of each EC metric without applying the channel selection method, averaged across all seven frequency bands.

Illustrations of selected channels using normalized importance of channels based on effective connectivity

Figures 6-8 illustrate the topographic maps of electrodes selected from datasets 1, 2, and 3, respectively. Figure 8 presents topographical maps of EEG channels selected from

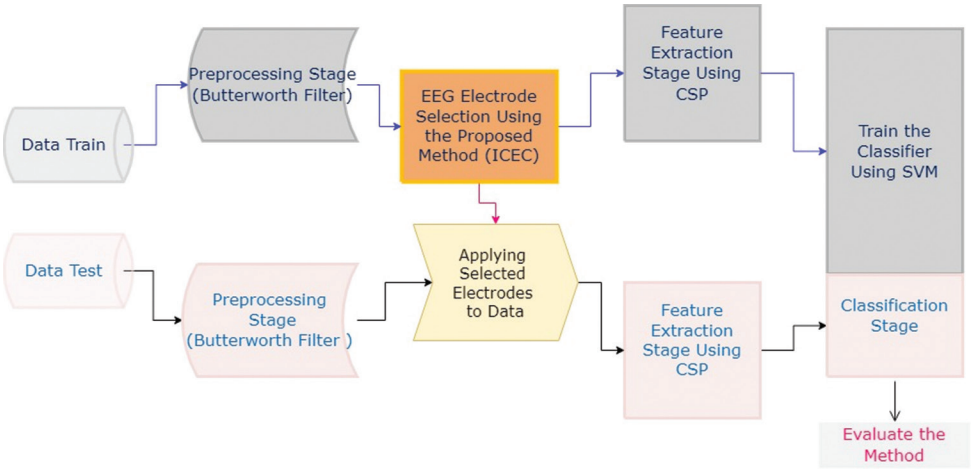

Figure 4: Main framework for evaluating the proposed electroencephalography channel selection method using common spatial pattern in the feature extraction stage and support vector machine for classifying. EEG – Electroencephalography; ICEC – Importance of channels based on effective connectivity; CSP – Common spatial pattern

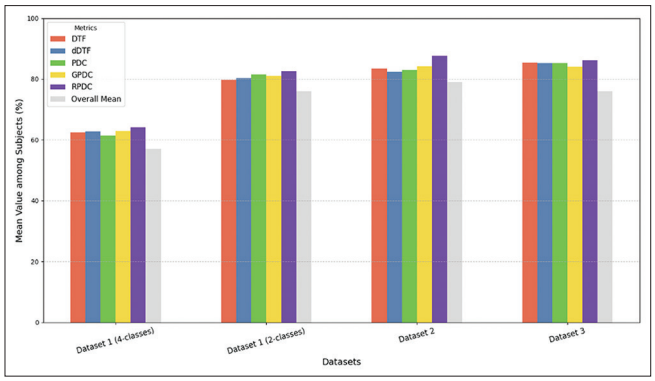

Figure 5: Comparison of mean classification accuracy across subjects for three datasets (dataset 1: 4-class and 2-class tasks; dataset 2; dataset 3). Bars represent performance with channel selection using different effective connectivity measures (directed transfer function [DTF], direct DTF, partial directed coherence [PDC], generalized [PDC], and renormalized [PDC]), along with the mean accuracy obtained without channel selection. DTF – Directed transfer function; dDTF – Direct directed transfer function; PDC – Partial directed coherence; GPDC – Generalized partial directed coherence; RPDC – Renormalized partial directed coherence

dataset 3, showcasing the spatial distribution of EC (ICEC) values for participants "aa," "al," "av," "aw," and "ay." A color gradient is used to represent the prominence of the channels, transitioning from red (higher prominence) to blue (lower prominence). The maps highlight the regions of the scalp with the most significant EC, with each participant's analysis corresponding to a specific combination of EC metrics and frequency bands: DDTF in the high-beta band, DTF in the theta band, RPDC in the mu band, and RPDC or DTF in the 29–40 Hz band. These visualizations emphasize the individual variability in connectivity patterns and the distinct regions of neural activity identified by the proposed ICEC criterion, providing insights into the key channels that contribute most to classification accuracy. Figures 6 and 7 also illustrate topographical maps of selected EEG channels from datasets 1 and 2.

Two distinct topographies of selected channels in Figure 6 using our proposed method are presented for each participant from dataset 1. The top illustration for each participant depicts the importance of EEG channels in the 4-class MI task (imagining the movement of the left hand, right hand, tongue, and foot), while the bottom illustration represents the importance of EEG channels in the 2-class MI task (imagining the movement of the left hand and right hand), with the exception of subject 9. Comparing the channels with the highest ICEC values shows that similar brain regions are active in both the 2-class and 4-class tasks. However, in the 4-class task, these regions are more extended, indicating a broader involvement of the brain when the number of imagined movements increases. This suggests that while certain regions remain consistently important across tasks, the complexity of the 4-class task recruits additional areas, reflecting the increased cognitive demand associated with distinguishing between more MI classes.

Figure 9 visualizes the EC (RPDC) interactions among EEG electrode nodes within the theta frequency range for a single trial (user a03, dataset 1). Each subplot represents the connectivity patterns at 500 ms intervals over a 3-second timeframe. The size of each electrode indicates its ICEC measure, highlighting the most influential electrodes in terms of EC. The strength and direction of the connections are represented by the links between the nodes, with thicker and darker lines indicating stronger interactions. The visualizations illustrate the temporal evolution of key electrode interactions during the trial.

We examine the effect of increasing the number of selected electrodes based on the ICEC measures on classification accuracy across datasets and tasks [Figure 10], Figure 10a and b regarding dataset 1 and Figure 10c and d representing dataset 2 and 3. The results show that after selecting a certain number of electrodes, accuracy significantly improves and then continues to increase slightly, maintaining consistent performance. This trend highlights the effectiveness of selecting key electrodes identified by the ICEC criterion in achieving optimal classification outcomes. For example, in Figure 10c, for participant "g," the accuracy starts at approximately 0.6 with 10 selected electrodes and increases significantly to around 0.85 when 30 electrodes are selected. Beyond this point, the accuracy stabilizes with only slight improvements as more electrodes are added. Similarly, in Figure 10d, for participant "aa," the accuracy begins at around 0.5 with 10 selected electrodes, rises significantly to approximately 0.9 by the time 40 electrodes are selected, and remains stable with minor fluctuations thereafter. These trends highlight that selecting.

Key electrodes not only improve classification performance but also increase accuracy while significantly reducing the number of channels, thereby lowering data dimensionality.

Comparison with other methods

To evaluate our proposed method, we compared its results on three well-known global datasets with other state-of-the-art CSP-based methods. These results are shown in Tables 1 and 2. In Table 1, we compared the proposed method applied to dataset 1 (right hand vs. left hand) with 3 other channel selection methods (SCSP1, SCSP2, and IBGSA) and with the results of 2 other classification methods that do not make use of channel selection. The proposed method demonstrates competitive performance compared to other techniques across various subjects. While the proposed method achieves the highest mean accuracy of 82% ± 13.1% with a lower standard deviation in selected channels (13), it closely aligns with methods such as SCSP1 (81.63% ± 13.7%) and SCSP2 (79.1% ± 15.6%) and surpasses IBGSA (76.25% ± 10%), as well as[16] 74.5% ± 15.1% and[15] 79.93% ± 14.1%. Notably, the reduced channel count highlights the efficiency of the proposed approach in maintaining high accuracy while simplifying the model,

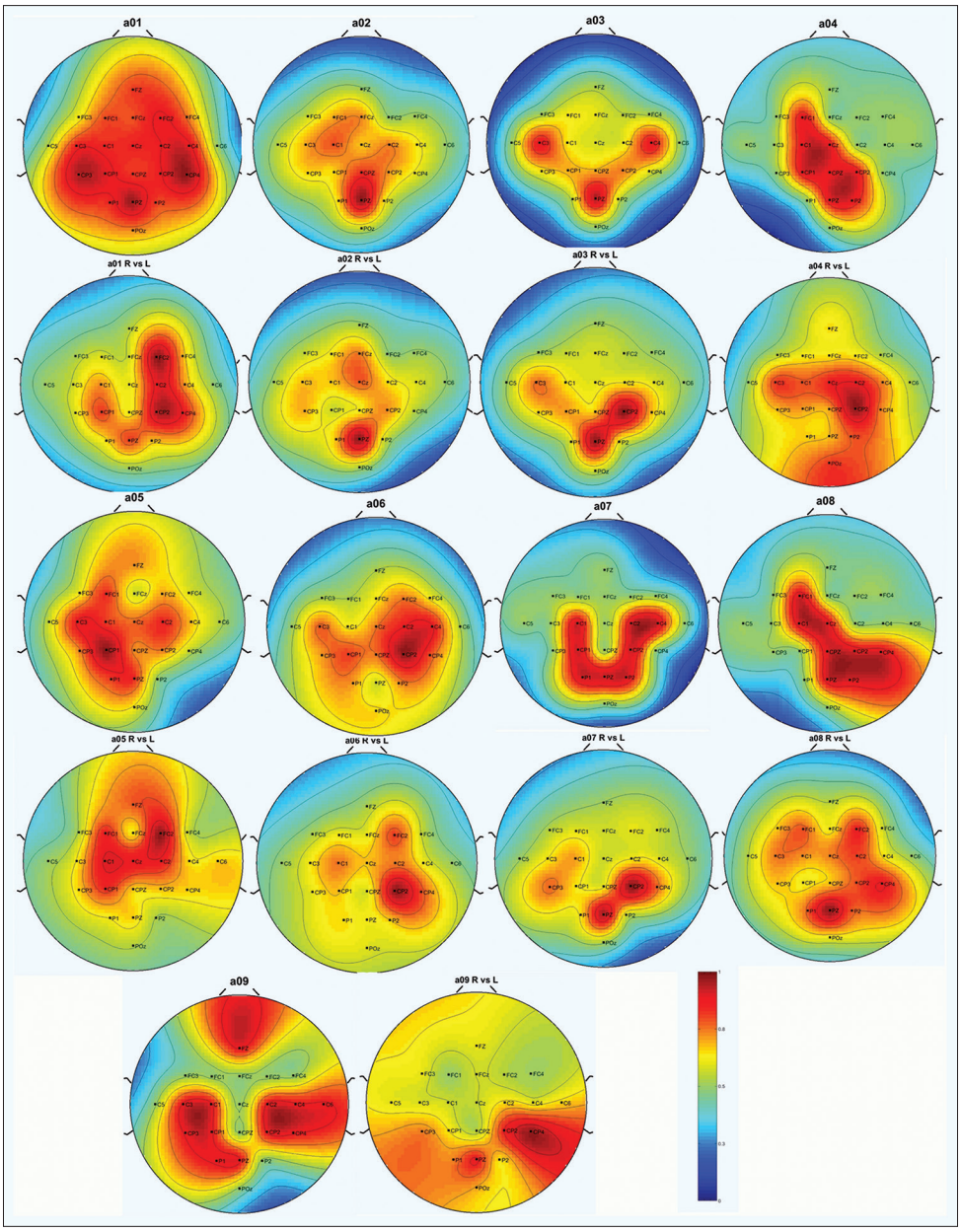

Figure 6: Two different topographies of selected channels using our proposed method for each participant (from dataset 1) are shown. For each participant, the top illustration represents the importance of electroencephalography (EEG) channels in the 4-class task (imagination of the movement of the left hand, right hand, tongue, and foot), while the bottom illustration represents the importance of EEG channels in the 2-class motor imagery task (imagination of the movement of the left hand and right hand) with the exception of subject 9

underscoring the robustness of the proposed method in optimizing classification accuracy with fewer resources.

Table 1 shows the comparison of the results of the proposed method applied to dataset 1 (right hand vs. left hand) with 5 other methods. The numbers in parentheses indicate the number of selected channels, and * denotes a statistically significant difference ($P < 0.05$) based on a paired *t*-test. Standard deviations are also presented alongside the average accuracies.

Table 2 shows the comparison of the proposed method's results with varying numbers of selected channels and their relative accuracies, applied to datasets 2 and 3 alongside five other methods. The numbers in parentheses indicate the number of selected channels, and * denotes a statistically significant difference ($P < 0.05$) based on a paired *t*-test. Standard deviations are also presented alongside the average accuracies.

Table 2 gives the results of using our proposed EEG channel selection method on datasets 2 and 3 and a comparison with 4 other methods (SFFS, improved SFFS, CSP-Rank, and BCS-CSP). As shown in Table 2, the proposed method (result 2) achieves the highest mean accuracy across both datasets (86.01% ± 7.5% for dataset 2 and 87.56% ± 7.90% for dataset 3) compared to

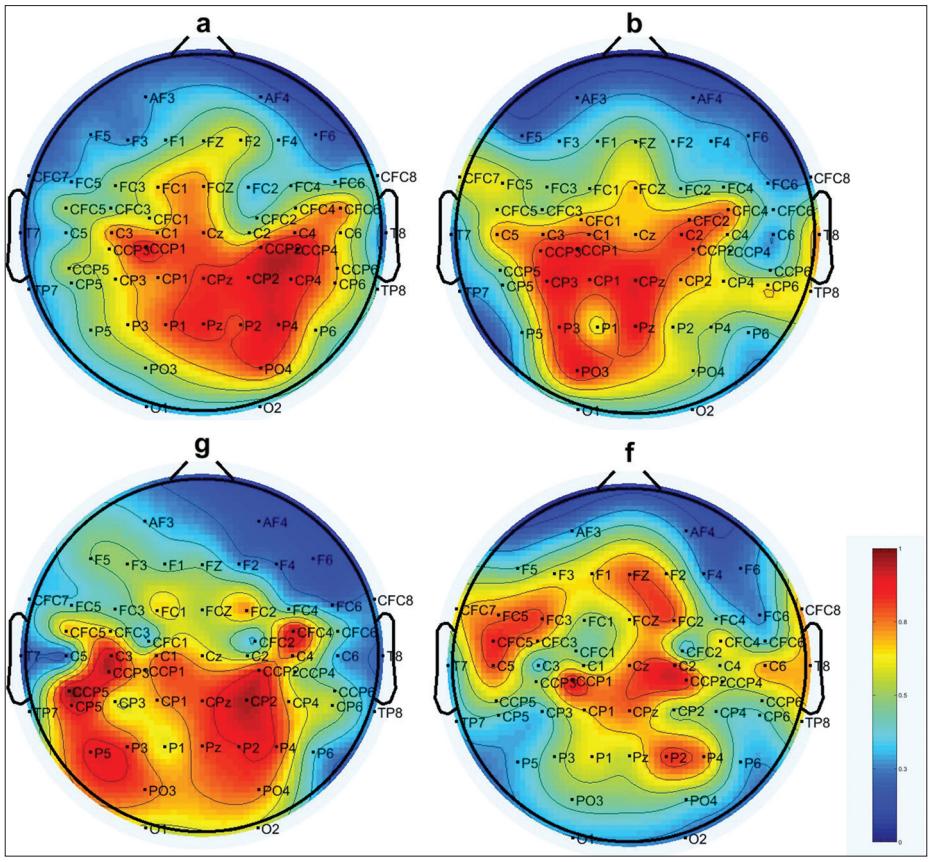

Figure 7: Topographical maps of channels selected from dataset 2 with 59 electroencephalography electrodes are shown. The color gradient, transitioning from red to blue, indicates decreasing prominence of the channels. To calculate the importance of channels based on effective connectivity for participants (a, b, f, and g), renormalized partial directed coherence (RPDC) was applied in the frequency range of 29–40 Hz, generalized partial directed coherence in the low-beta range, direct directed transfer function in the mu range, and RPDC in the high-beta range, respectively

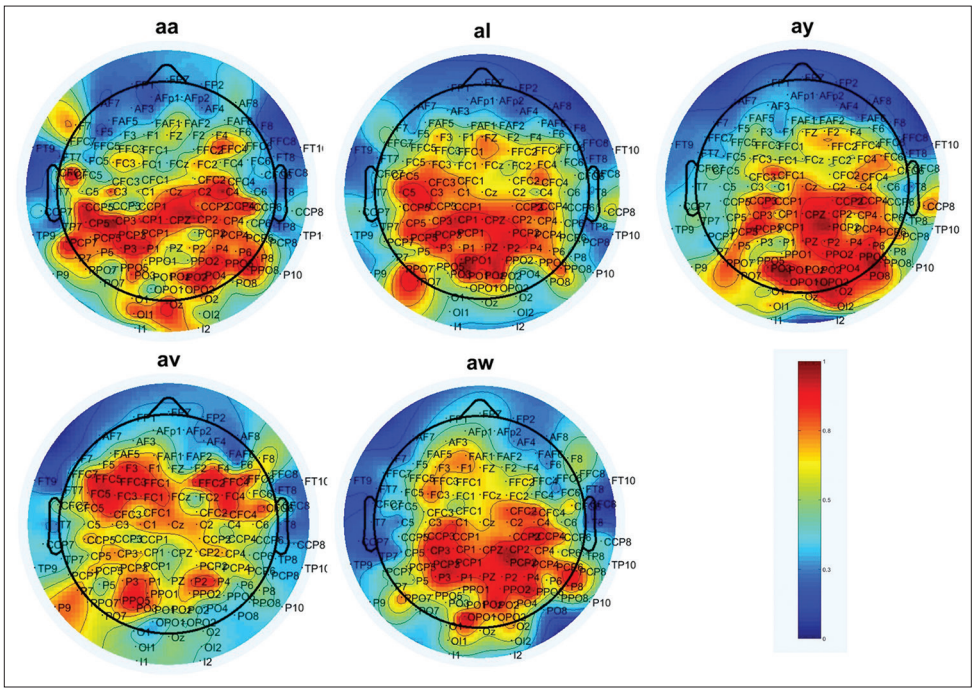

Figure 8: Topographical maps of channels selected from dataset 3 with 118 electroencephalography electrodes are shown. The color gradient, transitioning from red to blue, indicates decreasing prominence of the channels. To calculate the importance of channels based on effective connectivity for participants (aa, al, av, aw, and ay), we used direct directed transfer function (DTF) in the high-beta frequency band, DTF in theta, renormalized partial directed coherence (RPDC) in mu, DTF in 29–40 Hz, and RPDC in 29–40 Hz, respectively

Table 1: Comparison of results of the proposed method applied to dataset 1 (right hand vs. left hand) with 5 other methods

Subjects	Proposed method	SCSP1 Arvaneh *et al*., 2011[18]	SCSP2	IBGSA Ghaemi *et al*., 2017[33]	Gaur 2018[15]	Raza. H 2016[16]
a01	89.58 (11)	91.66 (13)	91.66 (13)	76.66 (9)	91.49	90.28
a02	63.19 (11)	67.36 (9)	60.41 (4)	76.66 (6)	60.56	54.17
a03	95.83 (16)	97.91 (14)	97.14 (12)	73.33 (7)	94.16	95.14
a04	76.39 (10)	72.22 (14)	70.83 (11)	73.33 (8)	76.72	65.97
a05	65.28 (11)	65.27 (11)	63.19 (9)	80 (11)	58.52	61.11
a06	75 (14)	66.67 (14)	61.11 (10)	73.33 (12)	68.52	65.28
a07	80 (19)	84.72 (19)	78.47 (15)	76.66 (15)	78.57	61.11
a08	98.61 (16)	97.22 (15)	95.13 (5)	80 (11)	97.01	91.67
a09	93.75 (10)	91.66 (10)	93.75 (5)	-	93.85	86.11
Mean	82±13.1 (13)	81.63±13.7 (13.2)	79.1±15.6 (9.3)	76.25±10* (10)	79.93±14.1 (22)	74.5±15.1* (22)

The numbers in parentheses indicate the number of selected channels, and * denotes a statistically significant difference (P<0.05) based on a paired t-test. Standard deviations are also presented alongside the average accuracies

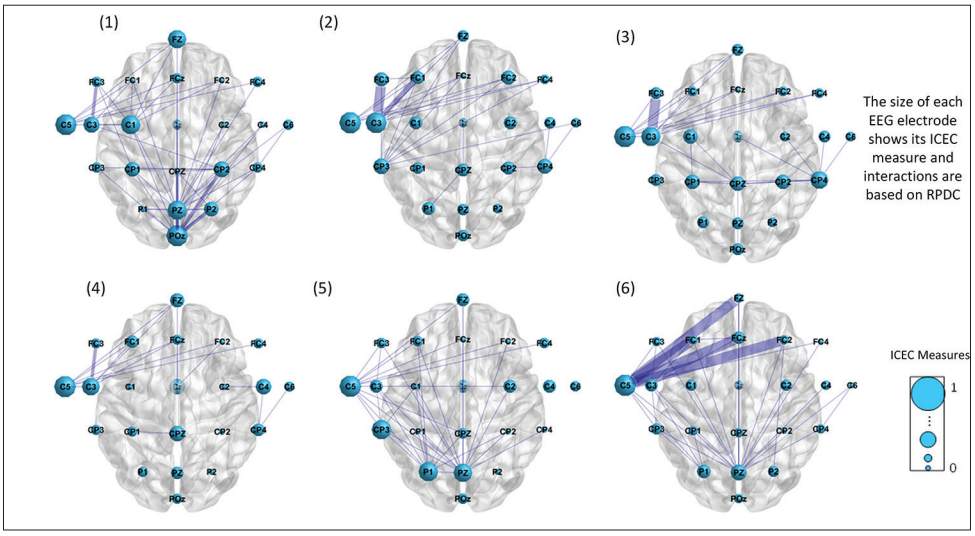

Figure 9: Effective Connectivity (renormalized partial directed coherence [RPDC]) interactions among electrode nodes in the theta frequency range. The images depict the differences in RPDC among sensors every 500 ms within a 3-second timeframe of a single trial (user a03, dataset 1). RPDC – Renormalized partial directed coherence; EEG – Electroencephalography; ICEC – Importance of channels based on effective connectivity

other methods. For the proposed method (result 2), most subjects demonstrated higher accuracies. For instance, in dataset 2, subjects "a" and "g" achieved accuracies of 89% (46 channels) and 97% (29 channels), respectively, which are significantly higher than other methods. Similarly, in dataset 3, subjects "aa" and "av" achieved accuracies of 84.03% (33 channels) and 96.43% (105 channels), respectively. The proposed method (result 2) significantly outperforms improved SFFS (67.25% ± 3.49%, $P < 0.05$) and SFFS (66.75% ± 9.83%, $P < 0.05$) in dataset 2, while also surpassing CSP-Rank (79.1% ± 6.21%) and BCS-CSP (83.75% ± 6.03%). Similarly, in dataset 3, the proposed method (result 2) shows statistically significant improvements ($P < 0.05$) over improved SFFS (83.32% ± 11.02%) and SFFS (84.22% ± 9.51%) and maintains better performance than CSP-Rank (86.3% ± 6.26%) and BCS-CSP (86.34% ± 8.30%). These results emphasize the robustness of the proposed method in achieving superior classification performance, with most subjects showing significant improvements ($P < 0.05$) and a reduced number of selected channels.

It is worth mentioning that, in our investigation, for a specific participant, electrodes with the highest ICEC amounts consistently maintained their ranks across all frequency ranges. For example, Figure 11 illustrates RPDC time-frequency representations for the electrodes C3 and CP3, which exhibit the highest ICEC values among all electrodes for participant "a08" from dataset 1. The plots depict interactions across six distinct frequency ranges, including theta, low-beta, Mu, high-beta, Gamma, and the broader 8–30 Hz band. These visualizations emphasize the strong and consistent EC between the selected electrodes, showcasing their dominant role in capturing relevant neural dynamics within the analyzed frequency bands.

Table 2: Comparison of the proposed method's results with varying numbers of selected channels and their relative accuracies, applied to datasets 2 and 3 alongside five other methods

Datasets	Subjects	Proposed method		Improved SFFS	SFFS	CSP-rank	BCS-CSP	Reg-CSP
		Result 1	Result 2	Qiu *et al*.[17]		Jin *et al*.[14]		Esfahani *et al*.[34]
Dataset 2	a	83.55 (21)	89 (46)	69 (6)	60 (9)	73 (5)	78.5 (12)	78 (16)
	b	79.53 (33)	79.53 (33)	63 (15)	66 (19)	77 (38)	77.5 (40)	72 (11)
	f	76.51 (39)	78.5 (46)	65 (8)	58 (19)	89.5 (47)	92 (33)	65 (18)
	g	96.1 (23)	97 (29)	72 (22)	83 (21)	77 (6)	87 (13)	75 (15)
	Mean	83.93 (25)±7.4	86.01 (29)±7.5	67.25 (12.7)±3.49*	66.75 (17.0)±9.83*	79.1 (24)±6.21*	83.75 (24.5)±6.03	72.5 (15)±5.57*
Dataset 3	aa	82.1 (19)	84.04 (33)	76.4 (27)	78.3 (26)	81.1 (80)	82.1 (105)	-
	al	94.64 (14)	96.43 (16)	94.3 (47)	93.6 (43)	94.3 (74)	95 (35)	-
	av	70.41 (22)	74 (105)	65 (18)	68.6 (18)	71.1 (64)	72.1 (72)	-
	aw	91.07 (24)	93 (36)	89.5 (27)	87.9 (20)	92.5 (27)	90.7 (68)	-
	ay	89.29 (53)	90.29 (53)	91.4 (35)	92.7 (35)	92.5 (68)	91.8 (111)	-
	Mean	85.50 (26.4)±8.58	87.56 (48.6)±7.90	83.32 (30.8)±11.02*	84.22 (28.4)±9.51*	86.3 (62.6)±8.93	86.34 (78.2)±8.30	-

The numbers in parentheses indicate the number of selected channels, and * denotes a statistically significant difference (P<0.05) based on a paired t-test. Standard deviations are also presented alongside the average accuracies

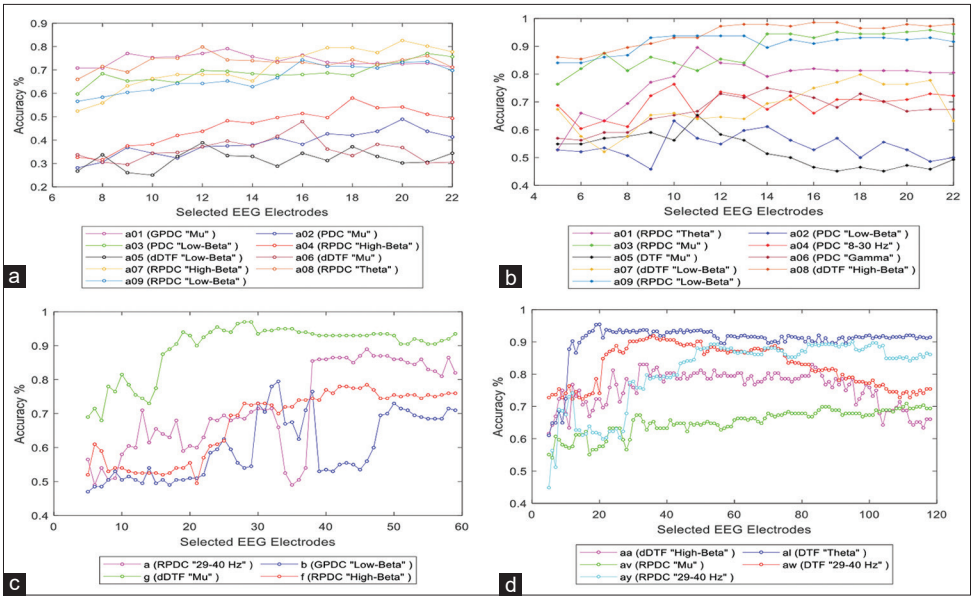

Figure 10: The accuracies associated with selected channels using our proposed method for dataset 1 (2-class [b] and 4-class [a] tasks), dataset 2 (c), and dataset 3 (d). Details of frequency ranges and effective connectivity metrics used are provided in the legends

Computational complexity and efficiency comparison

The ICEC-based method offers substantial computational efficiency compared to traditional channel selection approaches. Unlike wrapper-based methods, which require iterative classifier retraining and evaluation for each subset of channels, our method operates in an unsupervised fashion without involving the classifier during the selection stage. This significantly reduces the training overhead.

By leveraging EC metrics computed directly from the EEG signal using AMVAR modeling, our proposed method isolates the most informative channels in a single-pass pipeline. The resulting reduction in dimensionality not only speeds up feature extraction and classification but also lowers memory and computational demands. For example, across datasets, the average number of selected electrodes was reduced by up to 50%–60% without compromising classification performance.

Moreover, the use of frequency- and participant-specific EC profiles ensures targeted and minimal selection, enhancing generalizability and interpretability while avoiding the need for redundant computation. Overall, the ICEC framework provides a scalable, lightweight, and data-efficient solution suitable for real-time or resource-constrained neuroimaging applications.

Potential applications of the importance of channels based on the effective connectivity criterion

In this study, we employed the ICEC criterion to quantify the intensity of EC in each node (channel). We demonstrated how this criterion can be applied for channel selection, enabling improved system performance while reducing the number of required channels. In addition, we propose that the ICEC criterion has potential applications in other areas. For instance, in a previous study investigating the impacts of language-based circumstances on infants' brains,[35] we utilized the ICEC criterion for data visualization. In the present study, we further defined channel edge and weight matrices based on this criterion, specifically applying it to quantify EC in functional near-infrared spectroscopy data. We posit that the ICEC criterion can be broadly applied in contexts where either effective or FC is of interest, particularly in scenarios requiring decisions based on the degree of interaction between elements.

Conclusion

In this study, we introduced the ICEC criterion, a novel approach for quantifying EC in individual channels. Leveraging this criterion, we proposed an unsupervised channel selection method that considers the intensity of interactions among channels, leading to optimized sensor selection for classification tasks. Our method was rigorously evaluated on three widely recognized datasets across four categories, employing five EC metrics (PDC, GPDC, RPDC, DTF, and dDTF) and seven frequency ranges for comprehensive analysis. The results revealed consistent performance enhancements across all categories, particularly RPDC, with significant reductions in the number of selected electrodes, thereby demonstrating the efficiency of our approach. Among the frequency bands we analyzed, the high-beta range (18–30 Hz) and mu band (8–12 Hz) were the most consistently associated with

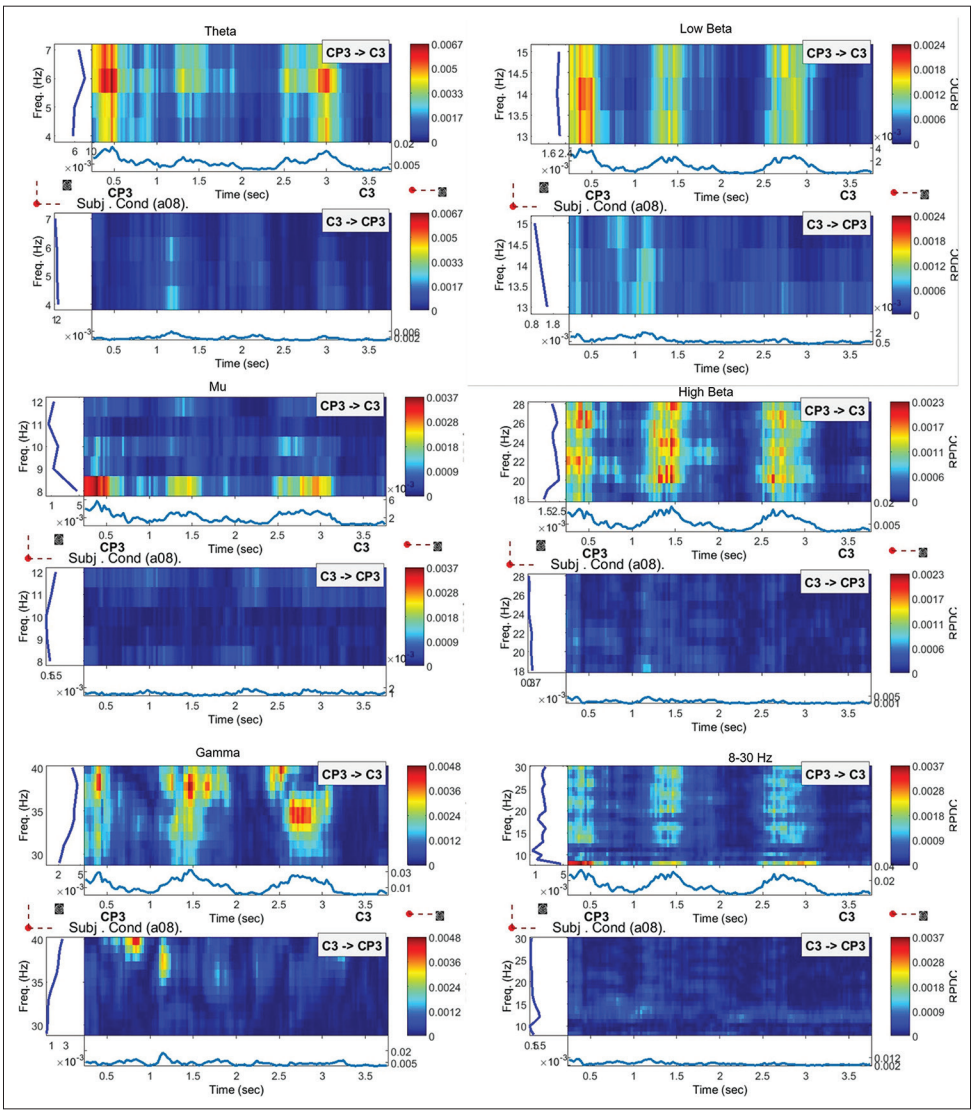

Figure 11: Renormalized partial directed coherence time-frequency illustrations of C3 and CP3 (which possess the highest importance of channels based on effective connectivity amounts compared to other electrodes) for participant "a08", dataset 1, across six frequency ranges

improved classification performance across participants, highlighting their significance in capturing discriminative connectivity patterns during MI tasks. Furthermore, our method outperformed traditional techniques such as SFFS, CSP-Rank, and BCS-CSP, achieving superior classification accuracies of 82%, 86.01%, and 87.56%, respectively. These outcomes validate the robustness and reliability of the ICEC-based channel selection strategy. Beyond improving classification outcomes, the ICEC criterion holds promise for broader applications, including data visualization and adaptability to other neuroimaging modalities. By adaptively selecting channels based on individualized connectivity patterns, our method ensures participant-specific, data-driven optimization of sensor selection and feature extraction, thereby contributing to advancements in neuroimaging analysis and related fields. Future work will explore its potential in diverse settings, further expanding its applicability and impact.

Ethical Approval

This study used publicly available datasets. All data were collected in accordance with relevant ethical guidelines and approved by the respective institutional review boards as reported in the original studies.

Availability of Data and Materials

The datasets analyzed in this study are publicly available and can be accessed from the original sources cited in the references.

Acknowledgments

This work was supported by Isfahan University of Medical Sciences under Grant 2401163.

Financial support and sponsorship

Nil.

Conflicts of interest

There are no conflicts of interest.

References

1. Khosla A, Khandnor P, Chand T. A comparative analysis of signal processing and classification methods for different applications based on EEG signals. Biocybern Biom Eng 2020;40:649-90.
2. Gu X, Cao Z, Jolfaei A, Xu P, Wu D, Jung TP, *et al.* EEG-based brain-computer interfaces (BCIs): A survey of recent studies on signal sensing technologies and computational intelligence approaches and their applications. IEEE/ACM Trans Comput Biol Bioinform 2021;18:1645-66.
3. Värbu K, Muhammad N, Muhammad Y. Past, present, and future of EEG-based BCI applications. Sensors 2022;22:3331.
4. Bazargani M, Tahmasebi A, Yazdchi M, Baharlouei Z. An emotion recognition embedded system using a lightweight deep learning model. J Med Signals Sens 2023;13:272-9.
5. Teplan M. Fundamentals of EEG measurement. Measurement science review. 2002;2:1.
6. Shah NA, Wusthoff CJ. How to use: Amplitude-integrated EEG (aEEG). Arch Dis Child Educ Pract Ed 2015;100:75-81.
7. Baig MZ, Aslam N, Shum HP. Filtering techniques for channel selection in motor imagery EEG applications: A survey. Artif Intell Rev 2020;53:1207-32.
8. Qi F, Wu W, Yu ZL, Gu Z, Wen Z, Yu T, *et al.* Spatiotemporal-filtering-based channel selection for single-trial EEG classification. IEEE Trans Cybern 2021;51:558-67.
9. Aich U, Saha A, Woźniak M, Ijaz MF, Singh PK. Schizophrenia detection from electroencephalogram signals using image encoding and wrapper-based deep feature selection approach. Sci Rep 2025;15:21390.
10. Abdumalikov S, Kim J, Yoon Y. Performance analysis and improvement of machine learning with various feature selection methods for EEG-based emotion classification. Appl Sci 2024;14:10511.
11. Sporns O. Brain connectivity. Scholarpedia 2007;2:4695.
12. Porro CA, Francescato MP, Cettolo V, Diamond ME, Baraldi P, Zuiani C, *et al.* Primary motor and sensory cortex activation during motor performance and motor imagery: A functional magnetic resonance imaging study. J Neurosci 1996;16:7688-98.
13. Edde M, Leroux G, Altena E, Chanraud S. Functional brain connectivity changes across the human life span: From fetal development to old age. J Neurosci Res 2021;99:236-62.
14. Jin J, Liu C, Daly I, Miao Y, Li S, Wang X, Cichocki A. Bispectrum-based channel selection for motor imagery based brain-computer interfacing. IEEE Trans Neural Sys Rehabil Eng 2020;28:2153-63.
15. Gaur P, Pachori RB, Wang H, Prasad G. A multi-class EEG-based BCI classification using multivariate empirical mode decomposition based filtering and Riemannian geometry. Expert Sys Appl 2018;95:201-11.
16. Raza H, Cecotti H, Li Y, Prasad G. Adaptive learning with covariate shift-detection for motor imagery-based brain–computer interface. Soft Comput 2016;20:3085-96.
17. Qiu Z, Jin J, Lam HK, Zhang Y, Wang X, Cichocki A. Improved SFFS method for channel selection in motor imagery based BCI. Neurocomputing 2016;207:519-27.
18. Arvaneh M, Guan C, Ang KK, Quek C. Optimizing the channel selection and classification accuracy in EEG-based BCI. IEEE Trans Biomed Eng 2011;58:1865-73.
19. Tiwari A, Chaturvedi A. A novel channel selection method for BCI classification using dynamic channel relevance. IEEE Access 2021;9:126698-716.
20. Settles B. Active Learning Literature Survey; 2009.
21. Seth A. Granger causality. Scholarpedia 2007;2:1667.
22. Baccala LA, Sameshima K. Brain connectivity. Methods in brain connectivity inference through multivariate time series analysis. CRC Press, Boca Raton 2014:1-9.
23. Bressler SL, Kumar A, Singer I. Brain synchronization and multivariate autoregressive (MVAR) modeling in cognitive neurodynamics. Front Syst Neurosci 2021;15:638269.
24. ndemann CM, Krause BM, Nourski KV, Banks MI, Veen BV. Multivariate autoregressive model estimation for high-dimensional intracranial electrophysiological data. Neuroimage 2022;254:119057.
25. Delorme A, Makeig S. EEGLAB: An open source toolbox for analysis of single-trial EEG dynamics including independent component analysis, J Neurosci Methods 2004;134:9-21.
26. Delorme A, Mullen T, Kothe C, Akalin Acar Z, Bigdely-Shamlo N, Vankov A, *et al.* EEGLAB, SIFT, NFT, BCILAB, and ERICA: New tools for advanced EEG processing. Comput Intell Neurosci 2011;2011:130714.

27. Mullen T. Source information flow toolbox (SIFT). Swartz Center Comput Neurosci. 2010;15:1-69.
28. Brockwell PJ, Dahlhaus R, Trindade AA. Modified Burg algorithms for multivariate subset autoregression, Statistica Sinica 2005197-213.
29. Brunner C, Leeb R, Müller-Putz G, Schlögl A, Pfurtscheller G. BCI competition 2008 – graz data set A, institute for knowledge discovery (Laboratory of Brain-Computer Interfaces). Graz Univ Technol 2008;16:1-6.
30. Tangermann M, Müller KR, Aertsen A, Birbaumer N, Braun C, Brunner C, *et al.* Review of the BCI competition IV. Front Neurosci 2012;6:55.
31. Blankertz B, Müller KR, Krusienski DJ, Schalk G, Wolpaw JR, Schlögl A, *et al.* The BCI competition. III: Validating alternative approaches to actual BCI problems. IEEE Trans Neural Syst Rehabil Eng 2006;14:153-9.9.
32. Martínez-Cancino R, Delorme A, Truong D, Artoni F, Kreutz-Delgado K, Sivagnanam S, *et al*. The open EEGLAB portal interface: High-performance computing with EEGLAB, Neuro Image 2021;224:116778.
33. Ghaemi A, Rashedi E, Pourrahimi AM, Kamandar M, Rahdari F. Automatic channel selection in EEG signals for classification of left or right hand movement in brain–computer interfaces using improved binary gravitation search algorithm. Biom Signal Process Control 2017;33:109-18.
34. Esfahani MM, Sadati H, Calhoun VD. Optimizing brain-computer interface performance: Advancing eeg signals channel selection through regularized csp and spea ii multi-objective optimization. arXiv preprint arXiv:2405.00721. 2024.
35. Abdollahpour N, Artan NS. Significant interactions in infant operculum regions when exposed to a bilingual environment: a resting-state fNIRS study. Neurophotonics. 2025;12:045012-
36. Abdollahpour N, Yazdchi M, Baharlouei Z. EEG Artifact Removal Based on Brain Dipoles' Regions Using ICA and Dipfit in Motor Imagery Tasks. In 2022 29th National and 7th International Iranian Conference on Biomedical Engineering (ICBME). IEEE; 2022. p. 22-7.